Engineering a potent receptor superagonist or antagonist from a novel IL-6 family cytokine ligand

Jun W. Kim[a], Cesar P. Marquez[b,c], R. Andres Parra Sperberg[a], Jiaxiang Wu[a,d], Won G. Bae[e], Po-Ssu Huang[a], E. Alejandro Sweet-Cordero[b,1], and Jennifer R. Cochran[a,f,1]

[a]Department of Bioengineering, Stanford University, Stanford, CA 94305; [b]Division of Hematology and Oncology, Department of Pediatrics, University of California, San Francisco, CA 94158; [c]School of Medicine, Stanford University, Stanford, CA 94305; [d]Tencent AI Lab, 518000 Shenzhen, China; [e]Department of Electrical Engineering, Soongsil University, 156-743 Seoul, Korea; and [f]Department of Chemical Engineering, Stanford University, Stanford, CA 94305

Interleukin-6 (IL-6) family cytokines signal through multimeric receptor complexes, providing unique opportunities to create novel ligand-based therapeutics. The cardiotrophin-like cytokine factor 1 (CLCF1) ligand has been shown to play a role in cancer, osteoporosis, and atherosclerosis. Once bound to ciliary neurotrophic factor receptor (CNTFR), CLCF1 mediates interactions to coreceptors glycoprotein 130 (gp130) and leukemia inhibitory factor receptor (LIFR). By increasing CNTFR-mediated binding to these coreceptors we generated a receptor superagonist which surpassed the potency of natural CNTFR ligands in neuronal signaling. Through additional mutations, we generated a receptor antagonist with increased binding to CNTFR but lack of binding to the coreceptors that inhibited tumor progression in murine xenograft models of nonsmall cell lung cancer. These studies further validate the CLCF1–CNTFR signaling axis as a therapeutic target and highlight an approach of engineering cytokine activity through a small number of mutations.

protein engineering | ligand–receptor interaction | yeast surface display

The interleukin-6 (IL-6) family of cytokines comprise four-helix bundle proteins that play an important role in inflammation, metabolism, and tissue regeneration (1). Members of this family include CNTF (ciliary neurotrophic factor), CLCF1 (cardiotrophin-like cytokine factor 1), LIF (leukemia inhibitory factor), OSM (oncostatin M), CT-1 (cardiotrophin 1), IL-6, IL-11, and IL-27 (1). Aberrant expression or dysregulation of these cytokines is widely found in cancer and autoimmune disease (2–6). Thus, therapeutic intervention directed at IL-6 and its receptors has been the focus of a number of preclinical and clinical studies (1, 7–14). In contrast, comparatively less work has been directed at targeting the CLCF1–CNTFR axis.

Human CNTF receptor (CNTFR) is a 373-amino-acid protein with a molecular weight of ∼41 kDa. Cytokine binding to the extracellular domain of CNTFR mediates recruitment and phosphorylation of coreceptors glycoprotein 130 (gp130) and leukemia inhibitory factor receptor (LIFR), triggering signaling cascades mediated by JAK-STAT, MAPK, and other pathways (15). CNTF, the first ligand discovered for CNTFR, was shown to have a direct neuroprotective effect on degenerating motor neurons in stress-induced conditions, both in cell culture and in a rodent model of axotomy-induced apoptosis (16, 17). The beneficial effect of CNTF on neuronal survival was further supported in a mouse model of neuronopathy with motor neuron degeneration (18). CNTF has also been found to play a role in the growth and support of cancer cells (16–22) including myeloma, glioma, neuroblastoma, and hepatic cancer. CLCF1 is underexplored in comparison to CNTF but is highly prominent in lung adenocarcinoma, where it is secreted by cancer cells and cancer-associated fibroblasts to promote tumor through both autocrine and paracrine signaling (23, 24). Furthermore, CLCF1 has also recently been shown to play a role in osteoporosis (25) and atherosclerosis (26). These studies highlight CNTFR and its ligands as targets for therapeutic intervention; a CNTFR agonist could potentially facilitate neuronal regeneration, while a CNTFR antagonist could inhibit this signaling axis for cancer or other disease treatment.

We used a combinatorial screening approach facilitated by yeast surface display to identify CLCF1 variants that altered receptor-mediated cell signaling and biochemical function in disparate ways. CLCF1 variants with significantly increased CNTFR affinity drove enhanced tripartite receptor complex formation and functioned as superagonists of cell signaling and axon regeneration. In contrast, an engineered CLCF1 ligand that bound CNTFR with high affinity but did not engage coreceptors gp130 or LIFR functioned as a receptor antagonist in a murine tumor xenograft model of nonsmall cell lung cancer (NSCLC).

Results

Engineering CLCF1 Variants with Increased CNTFR Affinity. A combinatorial protein engineering method known as yeast surface display (27) was used to generate CLCF1 variants with altered CNTFR binding properties. CLCF1 was displayed on the surface of yeast cells (28) as a fusion to the agglutinin mating protein Aga2p. Yeast cell surface expression levels of human CLCF1 and binding to a recombinant, soluble extracellular domain of human CNTFR fused to an antibody Fc domain (CNTFR-Fc) were quantified through antibody staining and analysis by flow cytometry

Significance

The interleukin-6 family of cytokines play an increasingly recognized role in inflammation, metabolism, and tissue regeneration. Cytokine binding to CNTFR triggers JAK-STAT, MAPK, and other associated pathways. From limited studies reported to date, CLCF1 has been implicated in lung cancer, osteoporosis, and atherosclerosis, identifying the CLCF1–CNTFR signaling axis as a therapeutic target for a number of diseases. To modulate multireceptor engagement to drive cell signaling, we used rational and combinatorial protein engineering methods to create two unique CLCF1 variants: one that promotes enhanced cell signaling in neuronal regeneration and one that blocks cell signaling to inhibit tumor progression. These studies highlight an approach of engineering cytokine activity to target the CLCF1–CNTFR signaling axis.

(*SI Appendix*, Fig. S1*A*). A first-generation library (~1×10^8 yeast transformants) was created via error-prone PCR to introduce random mutations into the CLCF1 gene. Iterative rounds of fluorescence-activated cell sorting (FACS) were used to isolate yeast-displayed CLCF1 variants exhibiting the top 0.5 to 1% binding signal for CNTFR-Fc (*SI Appendix*, Fig. S1 *B* and *C*). Screening stringency was increased in subsequent sort rounds by decreasing the concentration of CNTFR-Fc incubated with the library (*SI Appendix*, Fig. S2). After three rounds of sorting, a prominent consensus mutation (Q96R) emerged in the isolated yeast clones, along with a number of individual amino acid mutations appearing only one or two times (*SI Appendix*, Table S1). An apparent equilibrium binding affinity (K_d) of 8 ± 2 nM was measured between the yeast-displayed CLCF1 Q96R variant and recombinant CNTFR-Fc (*SI Appendix*, Fig. S3 *A* and *B*). The addition of amino acid mutations L86F or H148R slightly increased binding affinity for CNTFR-Fc by about twofold. In contrast, the affinity of wild-type (WT) CLCF1 was too weak to be quantified.

To identify permutations that further enhanced CNTFR binding affinity, a second-generation library was prepared by shuffling the DNA sequences of the enriched pool of CLCF1 variants using a technique known as staggered extension process (StEP) (29). Iterative rounds of FACS were again used to isolate yeast displaying the highest-affinity binders against CNTFR-Fc, first using equilibrium binding conditions followed by kinetic off-rate conditions to increase screening stringency (*SI Appendix*, Figs. S1 *D* and *E* and S2). After three sort rounds, permutations of six CLCF1 consensus mutations emerged (*SI Appendix*, Table S2). Currently, there is no reported structure of CLCF1, and thus to examine the selected mutations we used a deep learning-based prediction with a Rosetta energy function to create a structural framework (*Materials and Methods*). Structural homology between IL-6 family cytokines CLCF1, LIF, and IL-6 and between the receptors CNTFR and IL-6R were used to position CNTFR, LIFR, and gp130 (Fig. 1 *A* and *B*). Two of the prominent mutations (W169L and K180R) were located near the predicted receptor-binding interface of CNTFR. Y22C was located on the adjacent α helix (αA) where gp130 binding is predicted to occur. Two additional mutations (Q96R) and H148R were on the BC loop and N-terminal αD helix where LIFR is predicted to occur, with an additional mutation (L86F) on the αB helix distal from the predicted interface. A CLCF1 variant containing all six mutations (termed ss6) was constructed via cloning as this combination was not directly observed from library screening. Binding affinities of various combinations of CLCF1 consensus mutations were measured with yeast-displayed constructs, with ss4 and ss6 showing the tightest binding to CNTFR-Fc (apparent K_d values of 80 ± 20 pM and 60 ±10 pM, respectively; *SI Appendix*, Fig. S3 *C* and *D*).

CLCF1 Mutations Have Differential Effects on CNTFR, gp130, and LIFR Binding.
CLCF1 variants were produced and purified as soluble proteins in a bacterial expression system to further parse the effects of the six mutations enriched after the final round of sorting. Binding affinities of the soluble CLCF1 variants to CNTFR-Fc were measured using an enzyme-linked immunosorbent assay (ELISA)-based assay to capture and detect a ligand/receptor complex that has reached equilibrium. As observed with the yeast display binding assay, the affinity of WT CLCF1 and CNTFR-Fc was too weak to allow an apparent K_d to be measured (*SI Appendix*, Fig. S4 *A* and *B*). All CLCF1 variants showed significantly increased affinities for CNTFR-Fc compared with WT CLCF1, with the variants ss4 and ss6 again exhibiting the strongest affinities with apparent K_d values of 200 ± 40 pM and 120 ± 10 pM (Fig. 1*C* and *SI Appendix*, Fig. S4*B*).

Two independent approaches were used to characterize the ability of the CLCF1 variants to form receptor complexes. We first showed that binding of soluble WT CLCF1 to yeast-displayed

CNTFR can mediate complex formation with soluble gp130 (gp130-Fc) and LIFR (LIFR-Fc) (Fig. 1*D*). With this approach, CLCF1 variants containing mutations L86F, Q96R, and H148R and combinations thereof (rs1, rs2, rs3, and ss1) all exhibited higher binding signals to yeast-displayed CNTFR and soluble gp130-Fc as compared with WT CLCF1 (Fig. 1*E*), likely mediated through their increased binding affinities for CNTFR. Combining L86F, Q96R, and H148R with Y22C, W169L, and K180R to form variant ss6 decreased gp130 binding compared with WT CLCF1. All CLCF1 mutations showed higher binding to yeast-displayed CNTFR and LIFR-Fc compared with WT CLCF1 (Fig. 1*E*). In a second approach, an ELISA-based assay was used to measure receptor complex formation, where soluble CLCF1 variants were incubated with soluble CNTFR-His in the presence of soluble gp130-Fc. CLCF1 variants ss4 and ss6 exhibited significantly weaker binding to gp130 compared with WT CLCF1, with the addition of Y22C in ss6 further weakening the interaction (Fig. 1*F*). The presence of mutations L86F, Q96R, and H148R increased gp130 binding, with variant ss1 containing all three mutations showing the highest signal (Fig. 1*F*). When tested with soluble LIFR-Fc instead of gp130, again all CLCF1 mutations identified from library screening showed higher LIFR binding compared with WT CLCF1 (Fig. 1*G*).

The LIFR binding site in IL-6 family cytokines is characterized by an evolutionarily conserved FXXK motif located at the N terminus of αD helix, or site 3 (30). Alanine point mutations were introduced at positions F151 and K154 into WT CLCF1, ss1, and ss6 to create mutations WTAA, ss1AA, and ss6AA. The introduction of F151A and K154A mutations dramatically decreased LIFR binding in all three variants (Fig. 1 *F* and *G*). Collectively, these results indicate that L86F, Q96R, and H148R increase CNTFR, gp130, and LIFR binding, while Y22C, W169L, and K180R increase CNTFR and LIFR binding but decrease gp130 binding. Independent from these mutations, F151A and K154A specifically decrease LIFR binding without affecting gp130 binding.

CLCF1 ss1 Functions as a CNTFR Superagonist for Neuronal Regeneration.
Among the tested CLCF1 variants, ss1 (L86F, Q96R, and H148R) exhibits the highest gp130 and LIFR binding signal when complexed to CNTFR-Fc. Thus, we next examined if enhanced tripartite receptor complex formation driven by the increased affinity interaction between ss1 and CNTFR positively affects downstream signaling pathways as a more potent agonist. Rat embryonic cortical neurons (embryonic day 18 [E18]) were used as they offered a primary cell model. E18 cells were harvested and treated with CLCF1 or variant ss1, leading to time-dependent phosphorylation of STAT3 (Y705) and Erk (Fig. 2*A*). Treatment with ss1 elicited significantly higher levels of STAT3 and Erk phosphorylation and also led to prolonged Erk phosphorylation compared with WT CLCF1 treatment. The phosphorylation signal from ss1 treatment was also greater at lower concentrations, surpassing that of treatment with the related IL-6 family member CNTF, which has been shown to be effective in preclinical models and was included as a standard (Fig. 2*B*). Relative potency of ss1 was also demonstrated to be higher in human SH-SY5Y neuroblastoma cells compared with WT CLCF1 and CNTF (Fig. 2*B*), and effects were even greater than those observed in the E18 cells. Although ss1 was affinity-matured against human CNTFR, the high sequence homology between human and rat CLCF1 (89%) and CNTFR (94%) likely drives similar trends observed in E18 and SH-SY5Y cells.

In E18 and SH-SY5Y cells, all ss1 treatments led to higher cell survival under serum starvation conditions compared with an untreated control (Fig. 2*C*). While ss1 more effectively increased cell survival compared with WT CLCF1 and CNTF in both cell types, the differences of ss1 compared with CNTF were greater in SH-SY5Y cells, consistent with the phosphorylation data in
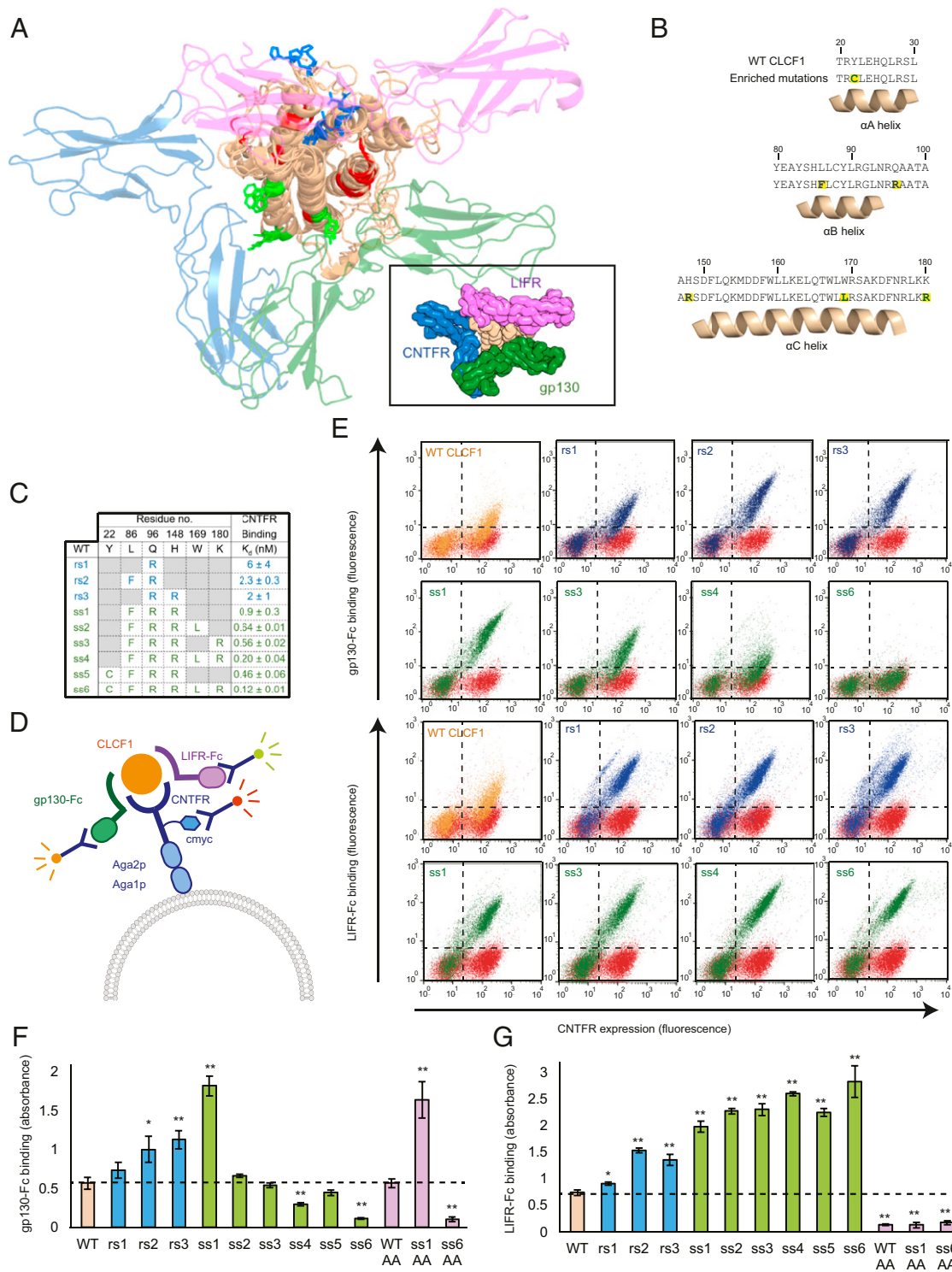
Fig. 1. (*A*) An ensemble of CLCF1 structures was generated using a deep learning-based prediction and a Rosetta energy function. Structural homology between CLCF1 and other IL-6 cytokines LIF and IL-6 (residues with similar properties shown in red) were used for positioning of the receptors CNTFR (blue), gp130 (green), and LIFR (pink), using the known crystal structures. The figure shows the locations of three mutations enriched from library 1 (blue) and three additional mutations enriched from library 2 (green). (*B*) Sequence of CLCF1 secondary structures where enriched mutations were located. Binding characterization of CLCF1 variants. (*C*) CNTFR-Fc binding affinities of soluble CLCF1 variants were determined using an ELISA-based assay. Individual binding curves can be found in *SI Appendix*. (*D*) Yeast-displayed CNTFR was used to form a complex with CLCF1 variants and either soluble gp130-Fc or LIFR-Fc coreceptors. CNTFR expression was detected by a labeled antibody against a C-terminal c-myc epitope tag. The binding of gp130-Fc or LIFR-Fc was detected by a labeled anti-Fc antibody. (*E*) Flow cytometry dot plots of gp130-Fc (100 nM) or LIFR-Fc (100 nM) binding to yeast-displayed CNTFR in the presence of soluble CLCF1 variants (2 nM). Red dots: CNTFR expression-only control. (*F* and *G*) Soluble CLCF1 variants (2 nM) were incubated with CNTFR-His (10 nM) and gp130-Fc (100 nM) or LIFR-Fc (100 nM). An ELISA-based assay was used to detect (*F*) gp130-Fc binding or (*G*) LIFR-Fc. Error bars represent ± SD, *n* = 3 per sample; *P < 0.05, **P < 0.01 vs. WT CLCF1. In *A*, *C*, and, *E–G* WT CLCF1: orange; blue: CLCF1 mutations identified from library 1; green: CLCF1 mutations identified from library 2; pink: F151 and K154 alanine point mutations.
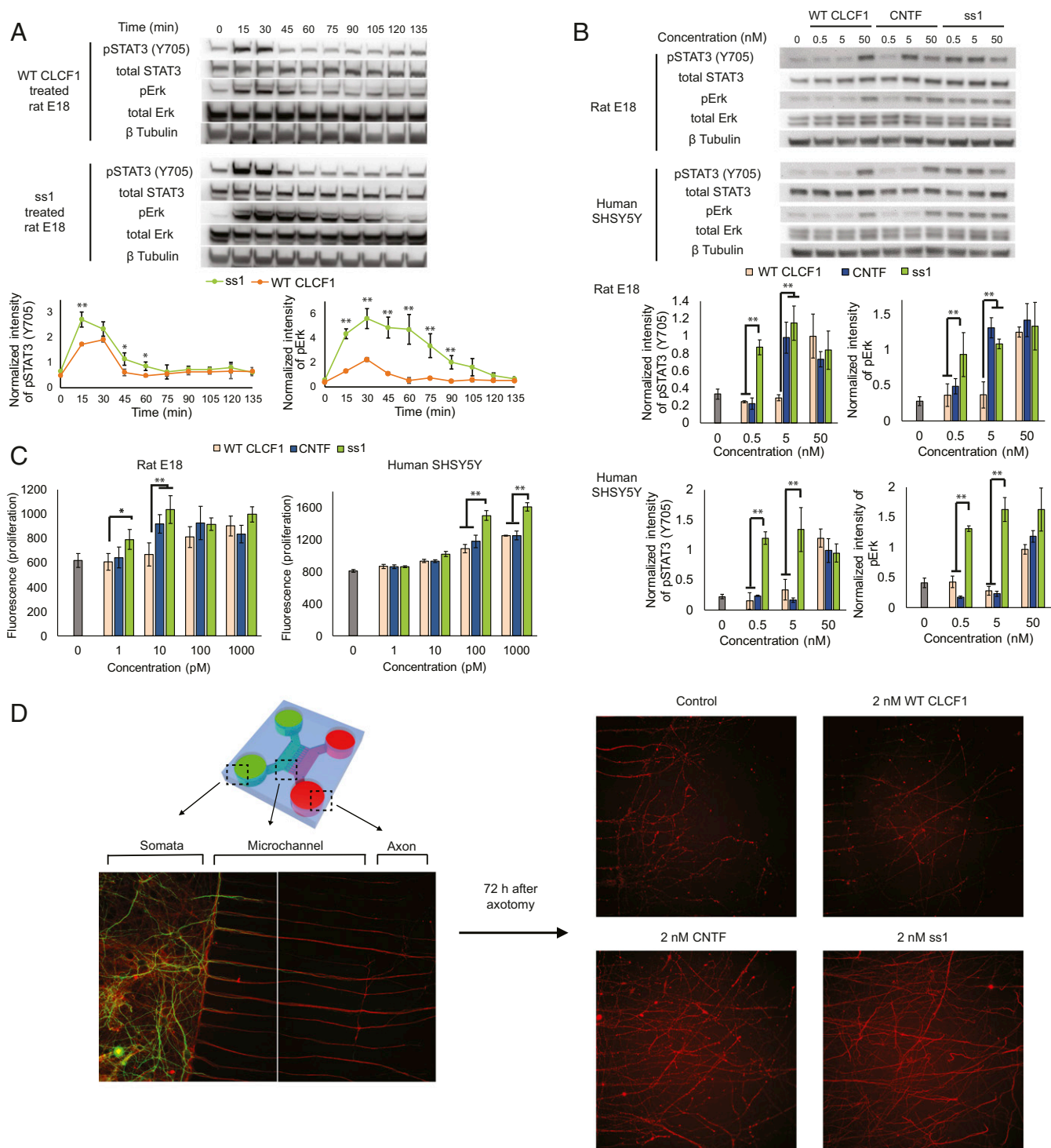
Fig. 2. ss1 treatment shows increased phosphorylation of STAT3 and Erk in rat embryonic cortical neurons (E18) and human SH-SY5Y cells and leads to higher cell survival and axon regeneration. (*A*) E18 cells were treated with WT CLCF1 (20 nM) or ss1 (20 nM) and analyzed at the indicated times posttreatment. Both treatments led to peak STAT3 (Y705) and Erk phosphorylation between 15 and 30 min with ss1-treated cells showing higher levels and, for pErk, prolonged signals. Error bars represent ± SD, *n* = 3 per sample; *P < 0.05, **P < 0.01 vs. WT CLCF1-treated group. The quantified intensity of the phosphorylated proteins was normalized against the intensity from the corresponding total proteins. (*B*) E18 cells and SH-SY5Y cells were treated with WT CLCF1, CNTF, or ss1 at varying concentrations for 20 min; ss1 treatment led to higher STAT3 and Erk phosphorylation in both cell lines. (*C*) E18 cells and SH-SY5Y were treated with WT CLCF1, CNTF, or ss1; after 72 h, ss1-treated cells showed increased number of metabolically active cells compared with the other treatments. Error bars represent ± SD, *n* = 3 per sample; *P < 0.05, **P < 0.01 vs. WT CLCF1-treated, CNTF-treated, or both groups. (*D, Left*) Four days after E18 cells were seeded in the somata chamber axons were found in the axon chamber (red: anti-MAP2; green: anti-Tau). (*D, Right*) Forty-eight hours after axotomy, axon regrowth was detected in the axon chamber. Both CNTF and ss1 treatment led to higher axon regrowth compared with control and WT CLCF1-treated samples.

Kim et al.

Fig. 2*B*. To test whether ss1 could also facilitate axonal regeneration, a microfluidic device with compartmentalization for isolating and directing the growth of injured axons was used to observe the effect of ss1 treatment on axon lesions in E18 cells (*SI Appendix,* Fig. S5) (31). Treatment with ss1 led to significantly higher regrowth of axons 72 h postlesion (Fig. 2*D*), compared with untreated control and WT CLCF1-treated cells. These data indicate that ss1, which has high affinity binding to CNTFR and drives enhanced complex formation between gp130 and LIFR, functions as a superagonist capable of increased neuronal cell signaling, proliferation, and axon regeneration compared with WT CLCF1.

CLCF1 ss6AA Functions as a CNTFR Antagonist in NSCLC Models.
CLCF1 variants with high affinity for CNTFR and decreased binding for gp130 or LIFR are expected to function as antagonists by blocking natural ligand binding to CNTFR and preventing activation of downstream cell signaling pathways. The CLCF1 variant ss6, containing F151A and K154A mutations (termed ss6AA), showed minimal binding for both LIFR and gp130 and the highest binding affinity for CNTFR-Fc (Fig. 1). Inhibition of CNTFR-Fc binding to soluble CLCF1, LIFR, or gp130 was measured upon the addition of ss6AA using an ELISA-based assay. Increasing concentrations of ss6AA decreased CLCF1, LIFR, and gp130 binding signals, showing that its addition prevents receptor complex formation with CNTFR-Fc in a competitive manner (Fig. 3*A*). To test whether ss6AA inhibits the downstream signaling pathways induced by WT CLCF1, the human NSCLC cell line A549 was incubated with WT CLCF1 and

different concentrations of CLCF1 variants. Cells treated with WT CLCF1 alone, or in combination with ss1, ss1AA, or ss6, stimulated STAT3 and gp130 phosphorylation. In contrast, the addition of ss6AA decreased WT CLCF1-mediated STAT3 and gp130 phosphorylation to background levels, indicating that effective inhibition of signaling is only achieved with mutations that confer lack of binding to LIFR and gp130 (Fig. 3*B*).

Next, the therapeutic efficacy of ss6AA was tested in a murine xenograft model of NSCLC. A549 cells were engrafted in two opposing flanks of NSG (NOD, SCID, gamma) immunodeficient mice. Primary tumors were allowed to grow to 100 mm^3 prior to treatment. The tumor-bearing mice were injected intraperitoneally with 1 mg/kg body weight of ss6AA or vehicle three times per week for 32 d. Administration of ss6AA led to significantly decreased tumor volume compared with the vehicle control (Fig. 3*C*). A substantial decrease in proliferation, detected by phospho-histone H3 (PH3), and an increase in apoptosis, detected by cleaved caspase-3 (CC3), were also observed in the tumor tissue after ss6AA treatment, as was a decrease in Erk phosphorylation (Fig. 3*D*). Similar effects were observed with human H23 cells, where tumor-bearing mice were treated with 1 mg/kg body weight with ss6AA or vehicle three times per week for 21 d (*SI Appendix,* Fig. S6 *A–C*). No significant changes in body weight were observed with treatment (*SI Appendix,* Fig. S6*D*), demonstrating that ss6A was generally well tolerated in the mice with this dosing regimen. Collectively, these data indicate that the increased binding affinity to CNTFR, concomitant with
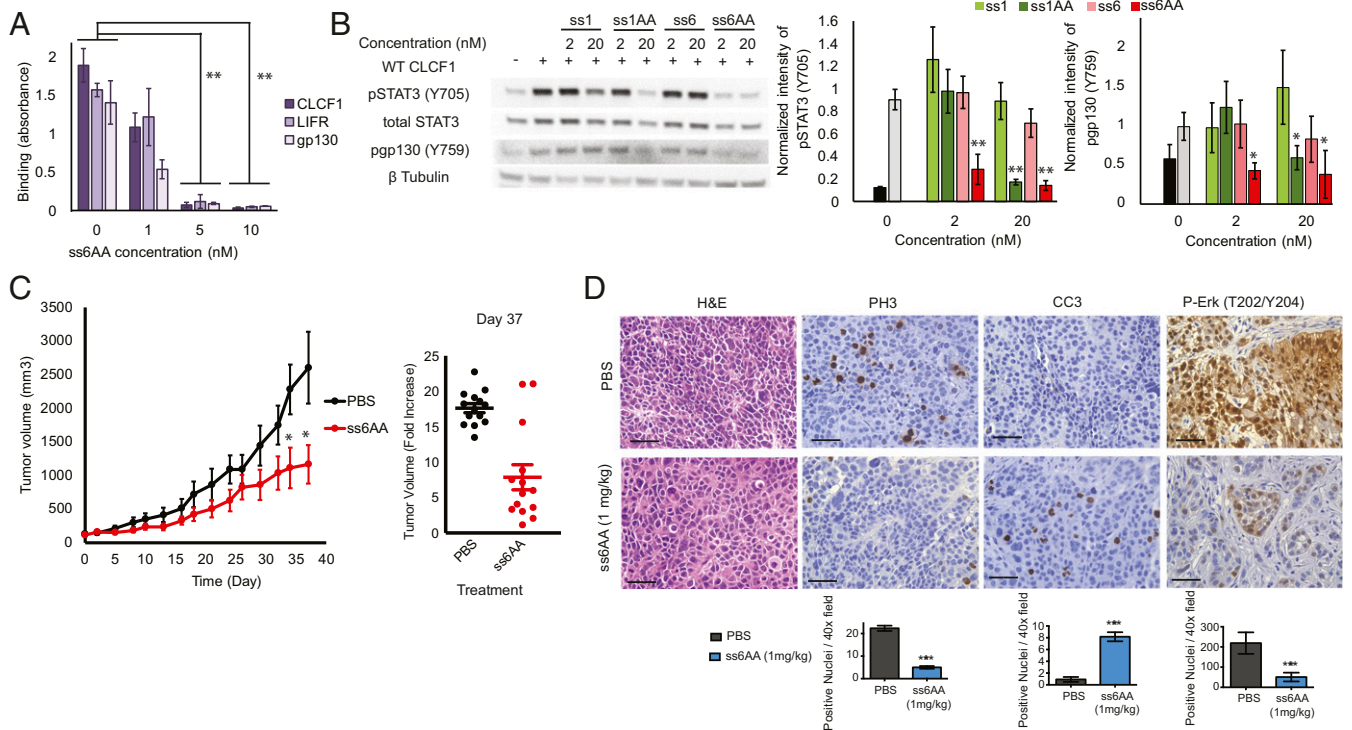
Fig. 3. ss6AA treatment inhibits receptor complex formation and STAT3 phosphorylation in vitro and NSCLC xenograft tumor growth in vivo. (*A*) CNTFR-Fc (2 nM) was incubated with the indicated concentrations of soluble ss6AA and WT CLCF1-His (20 nM), gp130-His (20 nM), or LIFR-His (20 nM). Binding to CNTFR-Fc was quantified with an anti-His antibody using an ELISA-based assay. At 5 nM and 10 nM concentrations ss6AA completely inhibits WT CLCF1-His, LIFR-His, and gp130-His binding to CNTFR-Fc. For assays detecting LIFR-His and gp130-His, 20 nM of CLCF1 was also included. (*B*) A549 human NSCLC cells were treated with 40 nM WT CLCF1 and CLCF1 variants at the indicated concentrations. ss6AA effectively inhibited STAT3 phosphorylation (Y705) and gp130 phosphorylation (Y759) induced by WT CLCF1. Black: nontreated control; gray: WT CLCF1-only control. Error bars represent ± SD, $n = 3$ per sample; *$P < 0.05$, **$P < 0.01$ vs. WT CLCF1-treated control. (*C*) Mice bearing A549 tumors in both flanks were treated with 1 mg·kg^{-1} body weight ss6AA ($n = 7$) or PBS alone ($n = 7$) three times per week for 3 wk. Error bars represent ± SE, $n = 7$ per treatment; *$P < 0.05$, **$P < 0.01$, ***$P < 0.001$. Vertical scatter plot shows individual tumor sizes on day 37. (*D*) Representative hematoxylin and eosin (H&E) staining and immunohistochemistry for PH3, CC3, and phospho-Erk (P-Erk) from A549 xenografts. (Scale bars, 50 μm.) Quantified values were compared using one-way ANOVA. Error bars represent ± SE.

diminished gp130 and LIFR binding, result in a CLCF1 variant that functions as a potent receptor antagonist.

Discussion

In this work, combinatorial protein engineering was used to create variants of the CLCF1 cytokine that functioned as receptor superagonists or antagonists. Random mutagenesis and high-throughput flow cytometry enabled isolation of yeast-displayed CLCF1 variants with increased binding affinity to CNTFR. Three mutations observed two or more times in the initial screen (L86F, Q96R, and H148R) were located in the region of CLCF1 known to interact with LIFR (30). The variant ss1, which combined all three mutations, bound with high affinity to CNTFR, mediated increased complex formation between CNTFR and gp130 or LIFR, and functioned as a potent CNTFR agonist. Two additional consensus mutations (W169L and K180R) enriched from the DNA shuffled library were located in a purported CNTFR binding region (32, 33). Combination of these mutations with L86F, Q96R, and H148R resulted in a CLCF1 variant, ss4, with retained high-affinity binding to CNTFR and increased LIFR interactions but reduced interaction with gp130. Y22C is located in a region of CLCF1 proposed to interact with gp130 (32). Addition of Y22C to create the variant ss6 further reduced gp130 engagement while retaining high-affinity interactions with CNTFR and LIFR. Finally, the introduction of two alanine mutations (F151A and K154A) into ss6 at locations evolutionarily conserved within site 3 of the IL-6 cytokine family (30) inhibited ligand-mediated interactions with LIFR. The resulting variant, ss6AA, binds with high affinity to CNTFR but does not engage gp130 or LIFR and thus functions as a competitive antagonist of WT CLCF1 in tumor cell signaling and murine xenograft models. Collectively, these results validate the power of library screens based on random protein mutagenesis. It would have proven difficult to accurately predict mutations that altered binding interactions between the CLCF1/CNTFR/gp130/LIFR complex, particularly since the first three mutations identified to increase CNTFR affinity were located in the purported LIFR binding domain.

Monoclonal antibodies are prominently used to modulate therapeutic targets for treating human disease. A ligand-based approach, like the one described here, can be beneficial given the complexity of activating a multireceptor complex with an antibody (34). CLCF1 variant ss1 was shown to be more potent in stimulating signaling in neuronal cells at lower concentrations compared with WT CLCF1 and CNTF, a related IL-6 cytokine family member. At concentrations where ss1 and CNTF stimulate cell signaling, both were more potent in a microfluidic-based axon regrowth assay compared with WT CLCF1. CNTF was previously evaluated for treating amyotrophic lateral sclerosis in two clinical trials with 570 and 730 patients. However, both trials reported no observable benefit of treatment, with severe adverse effects for doses over 5 μg/kg (35, 36). The half-life of CNTF after intravenous injection is only ~3 min, so subcutaneously (s.c.) administered CNTF was unlikely to have adequately reached its target cells at this low dose (37). Moreover, further studies found that CNTF has another binding partner, IL-6 receptor (IL-6R), which induces an acute-phase response on human liver cells, contributing to dose-limiting toxicity and suggesting that mono-specificity for CNTFR may improve the safety profile of CNTF (38, 39). Toward this end, researchers have attempted to create CNTF mutants with reduced IL-6R binding affinity, but these variants suffer from relatively weak CNTFR binding and hence have limited potency (40). WT CLCF1 binds with weaker affinity to CNTFR compared with CNTF and thus is a less potent agonist (41), a finding also confirmed in our studies. Importantly, CLCF1 does not bind to IL-6R and acts only through CNTFR. Therefore, we chose to engineer CLCF1 instead of using CNTF as a starting point, with the rationale that its lack of inherent IL-6R binding specificity could potentially mitigate toxic side effects (38, 42).

Phase III clinical trials were also conducted with recombinant CNTF as a treatment for obesity, after it was found that patients in neurodegeneration motor neuron disease trials experienced substantial weight loss (43). Ultimately, the treatment was not advanced due to modest efficacy and the finding that nearly 70% of patients developed antidrug antibodies after 3 mo of treatment. In a different approach, encapsulated human cells genetically engineered to secrete CNTF demonstrated statistically significant reduction in patients' macular telangiectasia without significant harmful side effects (44). In this case, ocular immune privilege is a well-described phenomenon which may prevent immunogenicity-induced side effects (45). Immunogenicity would need to be addressed for these CLCF1 variants if they were to move forward in clinical development, just as for all protein therapeutics, including human monoclonal antibodies. In many cases immunogenicity can be mitigated by mutation of predicted major histocompatibility complex epitopes or optimizing manufacturing processes to minimize aggregation (46).

Signaling pathways mediated by gp130-LIFR and their associated cytokines have been implicated in progression of a wide variety of cancers by directly promoting growth and by indirectly regulating inflammation (47). LIF, which directly activates gp130 and LIFR, is highly expressed by cancer cells and promotes tumor growth through autocrine signaling (48–50). Recently, LIF, like CLCF1, has been shown to mediate critical interactions between cancer cells and stromal cells, with LIF blockade and genetic *Lifr* deletion inhibiting tumor growth in pancreatic cancer (51). Other cytokines that activate gp130, such as IL-6 and OSM, have also been shown to drive tumor progression by promoting cell proliferation, survival, and cancer stem cell properties (4, 52), highlighting a broader role of IL-6 family of cytokines in cancer.

Interestingly, both soluble and cell membrane-constrained CNTFR can bind to CLCF1 and function as an agonist by interacting with coreceptors, gp130 and LIFR, to induce cell signaling (53–55). In previous studies, our group has shown that CLCF1 is highly overexpressed by cancer-associated fibroblasts in mouse models of lung cancer and in lung cancer patients and is a strong driver of autocrine and paracrine signaling leading to tumor progression (23, 24). We engineered a soluble CNTFR receptor decoy that was a potent inhibitor of tumor growth and progression in NSCLC, by engineering the decoy to have high affinity for CLCF1 and lack of binding to gp130 and LIFR (24). In our current study, we used engineered CLCF1 variants to further dissect the effects of coreceptor engagement on tumor cell signaling. Variant ss1AA, which blocks LIFR but not gp130 , inhibited CLCF1-mediated STAT3 phosphorylation at high concentrations. In contrast, variant ss6, which blocks gp130 but not LIFR engagement, did not inhibit CLCF1-mediated STAT3 phosphorylation at any concentration tested. Inhibition of complex formation with both gp130 and LIFR was required to effectively antagonize ligand-mediated cell signaling. We showed that CLCF1 variant ss6AA binds with high affinity to CNTFR and competitively inhibits WT CLCF1, LIFR, and gp130 binding to CNTFR. As a result, ss6AA subsequently inhibits CLCF1-mediated STAT3 and gp130 phosphorylation at low and high concentrations tested and functioned as an antagonist to inhibit tumor progression in two xenograft models of NSCLC.

In summary, using library screens and selective combination of identified mutations, we engineered unique CLCF1 variants that activate or inhibit CNTFR-mediated phenotypes in neurons or tumor cells, respectively. These results validate the CLCF1–CNTFR axis as a therapeutic target for neurodegenerative disease and cancer and show that cytokine-mediated tripartite receptor systems can be exploited to engineer potent ligand-based agonists and antagonists.

Kim et al.

Materials and Methods

Cells and Reagents. SH-SY5Y cells were kindly provided by Tobias Meyer, Stanford University, Stanford, CA. SH-SY5Y growth medium was Dulbecco's modified Eagle's media (DMEM, 11995; Fisher Scientific) with 10% fetal bovine serum (FBS) (26-140-079; Thermo Fisher Scientific) and 1% penicillin–streptomycin (15-140-122; Fisher Scientific). Embryonic rat cortical neurons (E18) were kindly provided by Lin Ning and Michael Lin, Stanford University. E18 cells were grown in Neurobasal (21103049; Thermo Fisher Scientific), 2% B27 (17504044; Thermo Fisher Scientific), 1% Glutamax (35050061; Fisher Scientific), and 1% FBS. Anti-CLCF1 antibody was purchased from Abcam (ab26125). Anti-His Hilyte Fluor 488 antibody was purchased from Anaspec (61250-H488) and anti-mouse Alexa 488 antibody was from Fisher Scientific (A11029). Anti-STAT3 (12640S), anti-phospho STAT3 (Y705) (9145S), anti-Erk1/2 (9102S), and anti-phospho Erk1/2 (9101) antibodies were from Cell Signaling Technology. Anti–β-tubulin antibody was from Covance (MMS-410P). Chicken anti-c-Myc antibody (A21281) and phospho(Tyr759)-gp130 antibody (PA564830) were purchased from Thermo Scientific and anti-chicken PE was purchased from Santa Cruz Biotechnology (sc-3730). Horseradish peroxidase (HRP)-conjugated anti-mouse (715-035-150) and anti-rabbit (711-035-152) antibodies were purchased from Jackson ImmunoResearch, and 1-Step Ultra TMB ELISA was from Thermo Scientific (34028).

Recombinant CLCF1 Production. Complementary DNA (cDNA) of the CLCF1 gene without the signal peptide sequence (residues L28 to F225) was cloned into the pET28b plasmid with an inducible lac promoter using BsaI and XhoI restriction sites and amplified in DH10B cells. For expression, purified plasmids were transformed into Rosetta gami cells. Cells in the logarithmic phase (optical density at 600 nm between 0.5 and 1) of growth was induced with 0.1 mM isopropyl-β-ᴅ-thiogalactoside in lysogeny broth media for 6 h at 37 °C. Induced cells were pelleted and resuspended in B-PER reagent (90084; Thermo Scientific) with lysozyme (0.1 mg/mL) and DNase I (5 U/mL) and incubated for 10 min at 37 °C. Lysate was centrifuged at $15,000 \times g$ for 5 min to pellet inclusion bodies. Inclusion bodies were solubilized in 60% double-distilled H_2O, 40% acetonitrile, and 0.1% trifluoroacetic acid containing 5 mM dithiothreitol. CLCF1 was purified with reverse-phase high-performance liquid chromatography using a Varian Prostar instrument and Vydac C18 column and was lyophilized and dissolved in 4 mM HCl. Linear gradients of 90% acetonitrile in water containing 0.1% (vol/vol) trifluoroacetic acid was used. Protein purity was further analyzed using sodium dodecyl sulfate polyacrylamide gel electrophoresis and quantified using a Nanodrop 2000 (Thermo Scientific).

Soluble CNTFR, LIFR, and gp130 Production. To produce His tag and antibody Fc domain fusion proteins of CNTFR, LIFR, and gp130, cDNA of CNTFR (M1-S342), LIFR (M1-S534), and gp130 (M1-S619) genes were cloned into the pAdd2 plasmid and amplified in DH10B cells. For expression, purified plasmids were transformed into Human Embryonic Kidney 293 (HEK 293) cells using polyethylenimine (PEI) (23966-2; Polysciences). Briefly, PEI was dissolved in endotoxin-free distilled H_2O (dH_2O) that had been heated to 80 °C to 1 g/L and stored at −80 °C as smaller aliquots. For 500-mL transfection volume HEK 293 cells were grown to 1×10^6 cells per mL in serum-free transfection medium (12338018; Thermo Fisher Scientific) at 37 °C in 5% CO_2. One-half milligram of purified DNA and 1 mL of PEI were dissolved in 10 mL of OptiPro Serum Free Media (12309-019; Thermo Fisher Scientific) each, then mixed immediately. After 15 min the solution was added dropwise to 500 mL of HEK 293 cells. Transfected cells were culture for five additional days before media were collected. Fc fusions were purified from culture supernatant using protein A Sepharose (101142; Thermo Fisher Scientific). His tag fusions were purified using Ni-NTA agarose (30210; Qiagen).

Preparation of Yeast-Displayed CLCF1 Libraries. DNA encoding human CLCF1 without the signaling peptide sequence (residues 28 to 225) was cloned into the pCTcon2 yeast display plasmid using NheI and BamHI restriction sites (56). Library 1 was created by error-prone PCR using the CLCF1 domain as a template, and mutations were introduced by low-fidelity Taq polymerase (50-811-694; New England Biolabs) and 55 mM MgCl$_2$. Separate PCR reactions were performed using different concentrations of MnCl$_2$ (0, 0.01, 0.05, 0.1, and 0.5 mM) (57). Products from these reactions were purified using gel electrophoresis. Purified mutant cDNA and linearized plasmid were electroporated into EBY100 yeast, where they were assembled in vivo through homologous recombination. Library size was estimated to be 8.1×10^7 by dilution plating. A second library was prepared using StEP (58). Twenty nonrepeating sequences were selected randomly from the population isolated in the final sort round of sorting of library 1. One nanogram of each of the templates was combined with the final concentrations of 0.15 μM of

each primer, 1× PCR buffer (B9004S; New England Biolabs), 200 μM 2′-deoxynucleoside 5′-triphosphate mix, 1.5 mM MgCl$_2$, and 2.5 U Taq polymerase in sterile dH_2O to 50 μL. The extension protocol was run for 100 cycles using the following parameters: 94 °C for 30 s (denaturation) and 55 °C for 10 s. Products from these reactions were purified using gel electrophoresis. Purified mutant cDNA and linearized plasmid were electroporated in EBY100 yeast. Library size was estimated to be 7.4×10^7 by dilution plating.

Library Screening.

Library 1. Yeast displaying high-affinity CLCF1 variants were isolated from the library using FACS. FACS rounds for the randomly mutagenized library were performed using equilibrium binding sorts where yeast were incubated at room temperature in phosphate-buffered saline (PBS) with 1 mg/mL bovine serum albumin (BSA) (PBSA) with the following concentrations: for sort 1, 20 nM CNTFR-Fc for 3 h; for sort 2, 2 nM CNTFR-Fc for 6 h; for sort 3, 0.5 nM CNTFR-Fc for 12 h. After incubation with CNTFR-Fc, yeast were pelleted, washed, and resuspended in PBSA with 1:500 ratio of chicken anti-c-Myc for 30 min at 4 °C. Yeast were then washed and pelleted, and secondary labeling was performed on ice for 30 min using PBSA with 1:100 dilution of goat anti-chicken PE and mouse anti-His HiLyte Fluor 488. Labeled yeast were sorted by FACS using a BD Aria II flow cytometer (Stanford FACS Core Facility) and BD FACSCalibur. Sorts were conducted such that the 0.5 to 1% of clones with the highest CLCF1 binding/c-Myc expression ratio were selected, enriching the library for clones with the highest binding affinity to CLCF1. Sorted yeast clones were propagated, induced for CLCF1 expression, and subjected to further rounds of FACS. After the last screening round, plasmid DNA was recovered using a Zymoprep kit (D2004; Zymo Research Corp.), transformed into DH10B electrocompetent cells, and isolated using a plasmid miniprep kit (K0503; Thermo Fisher Scientific). Sequencing was performed by MCLAB. Samples were analyzed on a FACSCalibur, and data were analyzed using FlowJo software (Tree Star Inc.).

Library 2. Yeast displaying CLCF1 variants with further increased receptor binding affinity were isolated from the library prepared via StEP. FACS rounds for library 2 were performed using a single round of equilibrium binding screening using 0.5 nM CNTFR-Fc followed by two rounds of kinetic off-rate sorts. For kinetic off-rate sorts, yeast were incubated with 2 nM CNTFR-Fc for 2 h at room temperature, after which cells were washed twice to remove excess unbound CNTFR-Fc and resuspended in PBSA containing 20 nM WT CLCF1 to render unbinding events irreversible. For the length of the unbinding steps, 10-h and 24-h incubation times were used. Yeast were then labeled with secondary antibodies and sorted by FACS following the protocol described above.

Computational Modeling of the CLCF1/CNTFR/LIFR/gp130 Complex. CLCF1 ensemble structures were generated by a distance-assisted protein folding pipeline. A deep convolutional network with residual connections was adopted to predict interresidue geometries (59). Pairwise distance between C-beta atoms and various types of dihedral angles consisted by C-beta/C-alpha/N/O atoms were predicted for all of the interresidue pairs. Such predictions were then converted into differentiable energy terms via spline approximation to enhance Rosetta's energy functions. Randomly initialized structures were optimized by centroid-level MinMovers, followed by the full-atom fast-relaxation, with prediction-based energy terms included. Afterward, an extra round of fast relaxation was carried out with disulfide bond restraints imposed, to further refine the structure. A total of 5,000 modeled CLCF1 structures were generated, from which the 500 lowest-energy structures were selected by total Rosetta energy. Structures were further selected by disulfide energy (dslf_fal13), resulting in an ensemble of 20 lowest disulfide energy structures shown in figure (*SI Appendix*, Fig. S1F and Dataset S1). Solved crystal structures of mLIFR–LIF complex (Protein Data Bank [PDB] ID code 2Q7N) and IL-6–IL-6alphaR–gp130 (PDB ID code 1P9M) were used as templates for receptor positioning. Structural homology between IL-6 family cytokines CLCF1, LIF, and IL-6 were used to position receptors LIF, IL-6alphaR, and gp130. Namely, residues with similar properties were selected at homologous positions in the crystal structures and used for Calpha atom pair alignment with corresponding CLCLF1 residues using the PyMOL pair_fit command (shown in red, Fig. 1A). Finally, the three-dimensional structure prediction of CNTFR was carried out with the Phyre 2 server (Protein Homology/analogy Recognition Engine V 2.0) and was superimposed to the IL-6alphaR position (Dataset S2).

Yeast Cell Binding Assays. Yeast-displayed CLCF1 mutants were incubated with varying concentrations of CNTFR-Fc for 12 h at room temperature to reach equilibrium, followed by washing with PBSA and resuspension in PBSA with a 1:500 ratio of chicken anti-c-Myc for 30 min at 4 °C. Yeast were then washed and pelleted, and secondary labeling was performed on ice for

30 min using PBSA with a 1:100 dilution of goat anti-chicken PE and mouse anti-HIS HiLyte Fluor 488. The samples were then washed and analyzed by flow cytometry using an Accuri flow cytometer (BD Biosciences) and data were analyzed using FlowJo software.

To characterize the on-cell receptor complex-forming properties of the CLCF1 variants, cDNA encoding human CNTFR extracellular domain (residues A18 to S342) was cloned into the pCTcon2 plasmid using NheI and BamHI restriction sites and electroporated into EBY100 yeast. Yeast displaying CNTFR were incubated with 100 nM gp130-Fc or LIFR-Fc in the presence of different CLCF1 variants for 2 h at room temperature. This was followed by washing with PBSA and resuspension in PBSA with a 1:500 ratio of chicken anti-c-Myc for 30 min at 4 °C. Yeast were then washed and pelleted, and secondary labeling was performed on ice for 30 min using PBSA with a 1:100 dilution of goat anti-chicken PE and anti-mouse Alexa 488.

ELISA-Based Binding Assays. To quantify binding affinities of CLCF1 variants for CNTFR in cell-free conditions, different concentrations of soluble CLCF1 constructs were incubated with 2 nM CNTFR-Fc in PBSA for 12 h at room temperature. To capture the CLCF1/CNTFR-Fc complex the mixture was then added to 96-well plates coated with anti-mouse-Fc antibody for 1 h, followed by washing twice with PBS. Subsequently, the wells were incubated with 1:1,000 diluted anti-CLCF1 rabbit antibody for 2 h at room temperature then washed four times with PBS. The wells were incubated with 1:1,000 diluted HRP-conjugated anti-rabbit antibody for 2 h at room temperature and washed four times with PBSA. The 1-Step Ultra TMB ELISA reagent was used for signal detection by measuring absorbance at 450 nm with microplate reader (BioTek Synergy H1).

To quantify interaction between CLCF1 complexed with CNTFR-His and soluble gp130-Fc or LIFR-Fc, CLCF1 (2 nM) variants were allowed to interact with CNTFR-His (10 nM) and gp130-Fc (100 nM) or LIFR-Fc (100 nM) in BPBS for 12 h at room temperature. The mixture was then added to 96-well plates coated with rabbit anti-His antibody for 1 h followed by washing twice with PBS. Subsequently, the wells were incubated with 1:1,000 diluted HRP-conjugated anti-mouse-Fc antibody and developed and analyzed as described above.

Phosphorylation Assays. SH-SY5Y, E18, A549, and H23 cells were grown to 50% confluence in six-well plates. The cells were incubated in varying concentrations of CLCF1 constructs for the indicated times at 37 °C in 5% CO_2 then lysed with Nonidet P-40 buffer containing protease and phosphatase inhibitor mixture (Invitrogen). For detection of phospho-gp130 ProteoExtract Native Membrane kit (Millipore Sigma) was used enrich for the membrane proteins. Equal amounts of lysate were loaded on Bis-Tris gels and transferred onto nitrocellulose membrane. The membranes were probed with primary antibodies against total STAT3, phospho-STAT3 (Y705), phospho-gp130 (Y759), total Erk1/2, phospho-Erk1/2, and β-tubulin at room temperature for 1 h. The blots were then washed and probed with HRP-conjugated anti-rabbit or anti-mouse antibodies as appropriate. The blots were developed with SuperSignal West Femto Maximum Sensitivity Substrate (34095; Thermo Scientific). Chemiluminescence was detected using the ChemiDoc XRS System (Bio-Rad Laboratories). The intensities of the bands were quantified using ImageJ image analysis software. For normalization of phospho-STAT3 and phospho-gp130, quantified intensities of the phosphorylated proteins were divided by intensities from the total STAT3 or β-tubulin, respectively.

Cell Proliferation Assay. SH-SY5Y (5×10^3) and E18 (2×10^4) cells were seeded into 96-well microtiter plates and grown for 24 h in 100 μL of DMEM containing 10% (vol/vol) FBS, and serum starvation was induced by incubating for 24 h in DMEM with 0.1% BSA for SH-SY5Y and neurobasal with 0.1% BSA for E18. CLCF1 constructs were then added and incubated for 72 h at 37C°, 5% CO_2. Next, cell proliferation was measured by adding AlamarBlue reagent (DAL1025; Thermo Fisher Scientific) to each well and incubating for 1 h at 37 °C, 5% CO_2. Fluorescence was measured with a Synergy H4 microtiter plate reader (BioTek Instruments) at 560-nm excitation/590-nm emission. Error bars represent the SD of triplicate wells. Data were measured against negative control containing only media.

Microfluidic Culture Platform for In Vitro Axonal Injury Assay. Microfluidic culture devices that compartmentalize neurons were prepared as reported previously (31). Briefly, the polydimethylsiloxane (PDMS) and glass coverslips

were sterilized with 70% ethanol before use. The cleaned glass coverslips were immersed in sterile solution of 1.0 mg/mL poly(L-lysine) (PLL) in water for 24 h before use. Sealing the PDMS piece to the PLL-coated glass coverslip by conformal contact formed the enclosed channels; 3×10^6 cells/mL were added to each of the somal side of the chamber. To create axonal injury vacuum aspiration was applied in the axonal compartment for 5 s and it was refilled with media to monitor regrowth of axons. Anti-Tau antibody was used to detect axons and anti-MAP2 antibody was used to detect dendrites.

In Vivo Tumor Model. To generate murine NSCLC xenograft models, 1×10^6 H23 cells were injected s.c. in the two lower flanks of NSG mice (strain 005557; The Jackson Laboratory). Xenograft tumors were injected when mice were ~8 to 10 wk of age. The tumors were allowed to grow to on average 100 mm³, and mice were stratified into treatment arms based on average tumor size per group before dosing. ss1AA solubilized in PBS was administered at 1 mg per kg body weight three times per week via intraperitoneal injection for 21 d. The tumor volume was measured with digital calipers and calculated using volume $= 0.5 \times (length) \times (width)^2$. The A549 study was conducted in a similar manner but for 32 d. Both male and female mice were used for xenograft studies.

Ethics Statement. Mice were maintained and animal experiments performed in accordance with policies approved by the Stanford University Administrative Panel on Laboratory Animal Care (protocol no. 14625).

Histology and Immunohistochemistry. Tissue specimens were fixed in 10% buffered formalin for 24 h and stored in 70% ethanol until paraffin embedding. Five-micrometer sections were stained with hematoxylin and eosin or used for immunohistochemical studies. Immunohistochemistry was performed on formalin-fixed, paraffin-embedded tissue sections using a biotin–avidin method. Briefly, sections were deparaffinized in xylene and rehydrated in ethanol. Standard sodium citrate, pH 6.0 buffered antigen retrieval was performed for 15 min prior to 3% H_2O_2 quenching for 10 min of endogenous peroxidase activity. Blocking and antibody dilutions were made in 5% normal goat serum (Vector Labs) in Tris-buffered saline containing 0.1% Triton X-100 (Sigma) and incubated overnight at 4 °C in a humidified chamber. The following antibodies were used (at indicated dilutions): P-Erk1/2 (4370, 1:400; Cell Signaling), PH3 (9701, 1:200; Cell Signaling), and CC3 (9661, 1:200; Cell Signaling). Sections were developed with 3,3′-diaminobenzidine peroxide substrate (642238; Abcam) and counterstained with hematoxylin. Pictures were taken using a Zeiss microscope (ZEISS) equipped with the Axiovision software (ZEISS). Analysis was performed using ImageJ software by measuring pixel units. All quantification analyses of immunohistochemistry staining were performed on three tumor specimens per treatment condition in three independent experiments. Data are displayed as mean per 40× field of view and error bars as SEM.

Statistical Analysis. Difference between groups in all experiments were examined for statistical significance using a two-tailed Student's t test. $P < 0.05$ was considered significant.

Data Availability. All data necessary for replication and relevant to this paper, including computational models of proteins, are included in the main text, *SI Appendix*, and Datasets S1 and S2.

1. S. Rose-John, Interleukin-6 family cytokines. *Cold Spring Harb. Perspect. Biol.* **10**, a028415 (2018).
2. K. Taniguchi, M. Karin, IL-6 and related cytokines as the critical lynchpins between inflammation and cancer. *Semin. Immunol.* **26**, 54–74 (2014).
3. C. A. Hunter, S. A. Jones, IL-6 as a keystone cytokine in health and disease. *Nat. Immunol.* **16**, 448–457 (2015).
4. D. J. Junk *et al.*, Oncostatin M promotes cancer cell plasticity through cooperative STAT3-SMAD3 signaling. *Oncogene* **36**, 4001–4013 (2017).

5. B. T. Gurfein et al., IL-11 regulates autoimmune demyelination. J. Immunol. 183, 4229–4240 (2009).

6. R. R. Meka, S. H. Venkatesha, S. Dudics, B. Acharya, K. D. Moudgil, IL-27-induced modulation of autoimmunity and its therapeutic potential. Autoimmun. Rev. 14, 1131–1141 (2015).

7. X. Li et al., LIF promotes tumorigenesis and metastasis of breast cancer through the AKT-mTOR pathway. Oncotarget 5, 788–801 (2014).

8. H. Zeng et al., Feedback activation of leukemia inhibitory factor receptor limits response to histone deacetylase inhibitors in breast cancer. Cancer Cell 30, 459–473 (2016).

9. M. S. Li et al., The Yin and Yang aspects of IL-27 in induction of cancer-specific T-cell responses and immunotherapy. Immunotherapy 7, 191–200 (2015).

10. R. Goldberg et al., Suppression of ongoing experimental autoimmune encephalomyelitis by neutralizing the function of the p28 subunit of IL-27. J. Immunol. 173, 6465–6471 (2004).

11. A. M. Weissmiller, C. Wu, Current advances in using neurotrophic factors to treat neurodegenerative disorders. Transl. Neurodegener. 1, 14 (2012).

12. N. A. Nicola, J. J. Babon, Leukemia inhibitory factor (LIF). Cytokine Growth Factor Rev. 26, 533–544 (2015).

13. C. A. Hunter, R. Kastelein, Interleukin-27: Balancing protective and pathological immunity. Immunity 37, 960–969 (2012).

14. K. Zhang et al., Ciliary neurotrophic factor delivered by encapsulated cell intraocular implants for treatment of geographic atrophy in age-related macular degeneration. Proc. Natl. Acad. Sci. U.S.A. 108, 6241–6245 (2011).

15. E. Lelièvre et al., Signaling pathways recruited by the cardiotrophin-like cytokine/cytokine-like factor-1 composite cytokine: Specific requirement of the membrane-bound form of ciliary neurotrophic factor receptor alpha component. J. Biol. Chem. 276, 22476–22484 (2001).

16. Y. Arakawa, M. Sendtner, H. Thoenen, Survival effect of ciliary neurotrophic factor (CNTF) on chick embryonic motoneurons in culture: Comparison with other neurotrophic factors and cytokines. J. Neurosci. 10, 3507–3515 (1990).

17. M. Sendtner, G. W. Kreutzberg, H. Thoenen, Ciliary neurotrophic factor prevents the degeneration of motor neurons after axotomy. Nature 345, 440–441 (1990).

18. M. Sendtner et al., Ciliary neurotrophic factor prevents degeneration of motor neurons in mouse mutant progressive motor neuronopathy. Nature 358, 502–504 (1992).

19. J. Weis et al., CNTF and its receptor subunits in human gliomas. J. Neurooncol. 44, 243–253 (1999).

20. H. Kuroda, T. Sugimoto, Y. Horii, T. Sawada, Signaling pathway of ciliary neurotrophic factor in neuroblastoma cell lines. Med. Pediatr. Oncol. 36, 118–121 (2001).

21. Z. J. Gu et al., A ciliary neurotrophic factor-sensitive human myeloma cell line. Exp. Hematol. 24, 1195–1200 (1996).

22. X. Hu et al., Ciliary neurotrophic factor receptor alpha subunit-modulated multiple downstream signaling pathways in hepatic cancer cell lines and their biological implications. Hepatology 47, 1298–1308 (2008).

23. S. Vicent et al., Cross-species functional analysis of cancer-associated fibroblasts identifies a critical role for CLCF1 and IL-6 in non-small cell lung cancer in vivo. Cancer Res. 72, 5744–5756 (2012).

24. J. W. Kim et al., Antitumor activity of an engineered decoy receptor targeting CLCF1-CNTFR signaling in lung adenocarcinoma. Nat. Med. 25, 1783–1795 (2019).

25. S. Nahlé et al., Cardiotrophin-like cytokine (CLCF1) modulates mesenchymal stem cell osteoblastic differentiation. J. Biol. Chem. 294, 11952–11959 (2019).

26. S. Pasquin et al., Cardiotrophin-like cytokine increases macrophage-foam cell transition. J. Immunol. 201, 2462–2471 (2018).

27. E. T. Boder, K. D. Wittrup, Yeast surface display for screening combinatorial polypeptide libraries. Nat. Biotechnol. 15, 553–557 (1997).

28. A. Angelini et al., Protein engineering and selection using yeast surface display. Methods Mol. Biol. 1319, 3–36 (2015).

29. H. Zhao, L. Giver, Z. Shao, J. A. Affholter, F. H. Arnold, Molecular evolution by staggered extension process (StEP) in vitro recombination. Nat. Biotechnol. 16, 258–261 (1998).

30. H. Plun-Favreau et al., Leukemia inhibitory factor (LIF), cardiotrophin-1, and oncostatin M share structural binding determinants in the immunoglobulin-like domain of LIF receptor. J. Biol. Chem. 278, 27169–27179 (2003).

31. A. M. Taylor et al., A microfluidic culture platform for CNS axonal injury, regeneration and transport. Nat. Methods 2, 599–605 (2005).

32. F. Rousseau et al., Ciliary neurotrophic factor, cardiotrophin-like cytokine, and neuropoietin share a conserved binding site on the ciliary neurotrophic factor receptor alpha chain. J. Biol. Chem. 283, 30341–30350 (2008).

33. D. Perret et al., Two different contact sites are recruited by cardiotrophin-like cytokine (CLC) to generate the CLC/CLF and CLC/sCNTFRalpha composite cytokines. J. Biol. Chem. 279, 43961–43970 (2004).

34. J. W. Kim, J. R. Cochran, Targeting ligand-receptor interactions for development of cancer therapeutics. Curr. Opin. Chem. Biol. 38, 62–69 (2017).

35. R. G. Miller et al., A placebo-controlled trial of recombinant human ciliary neurotrophic (rhCNTF) factor in amyotrophic lateral sclerosis. rhCNTF ALS Study Group. Ann. Neurol. 39, 256–260 (1996).

36. Anonymous; ALS CNTF Treatment Study Group, A double-blind placebo-controlled clinical trial of subcutaneous recombinant human ciliary neurotrophic factor (rHCNTF) in amyotrophic lateral sclerosis. Neurology 46, 1244–1249 (1996).

37. F. Dittrich, H. Thoenen, M. Sendtner, Ciliary neurotrophic factor: Pharmacokinetics and acute-phase response in rat. Ann. Neurol. 35, 151–163 (1994).

38. B. Schuster et al., Signaling of human ciliary neurotrophic factor (CNTF) revisited. The interleukin-6 receptor can serve as an alpha-receptor for CTNF. J. Biol. Chem. 278, 9528–9535 (2003).

39. H. Baumann et al., Reconstitution of the response to leukemia inhibitory factor, oncostatin M, and ciliary neurotrophic factor in hepatoma cells. J. Biol. Chem. 268, 8414–8417 (1993).

40. E. M. Wagener et al., The amino acid exchange R28E in ciliary neurotrophic factor (CNTF) abrogates interleukin-6 receptor-dependent but retains CNTF receptor-dependent signaling via glycoprotein 130 (gp130)/leukemia inhibitory factor receptor (LIFR). J. Biol. Chem. 289, 18442–18450 (2014).

41. R. Burger et al., Functional significance of novel neurotrophin-1/B cell-stimulating factor-3 (cardiotrophin-like cytokine) for human myeloma cell growth and survival. Br. J. Haematol. 123, 869–878 (2003).

42. A. J. Tormo et al., The cytokines cardiotrophin-like cytokine/cytokine-like factor-1 (CLC/CLF) and ciliary neurotrophic factor (CNTF) differ in their receptor specificities. Cytokine 60, 653–660 (2012).

43. M. P. Ettinger et al., Recombinant variant of ciliary neurotrophic factor for weight loss in obese adults: A randomized, dose-ranging study. JAMA 289, 1826–1832 (2003).

44. E. Y. Chew et al.; Macular Telangiectasia Type 2-Phase 2 CNTF Research Group, Effect of ciliary neurotrophic factor on retinal neurodegeneration in patients with macular telangiectasia type 2: A randomized clinical trial. Ophthalmology 126, 540–549 (2019).

45. A. W. Taylor, Ocular immune privilege. Eye (Lond.) 23, 1885–1889 (2009).

46. L. Yin, X. Chen, P. Vicini, B. Rup, T. P. Hickling, Therapeutic outcomes, assessments, risk factors and mitigation efforts of immunogenicity of therapeutic protein products. Cell. Immunol. 295, 118–126 (2015).

47. S. A. Jones, B. J. Jenkins, Recent insights into targeting the IL-6 cytokine family in inflammatory diseases and cancer. Nat. Rev. Immunol. 18, 773–789 (2018).

48. S. Peñuelas et al., TGF-beta increases glioma-initiating cell self-renewal through the induction of LIF in human glioblastoma. Cancer Cell 15, 315–327 (2009).

49. S. C. Liu et al., Leukemia inhibitory factor promotes nasopharyngeal carcinoma progression and radioresistance. J. Clin. Invest. 123, 5269–5283 (2013).

50. M. T. Wang et al., Blockade of leukemia inhibitory factor as a therapeutic approach to KRAS driven pancreatic cancer. Nat. Commun. 10, 3055 (2019).

51. Y. Shi et al., Targeting LIF-mediated paracrine interaction for pancreatic cancer therapy and monitoring. Nature 569, 131–135 (2019).

52. S. Kang, T. Tanaka, M. Narazaki, T. Kishimoto, Targeting interleukin-6 signaling in clinic. Immunity 50, 1007–1023 (2019).

53. T. Taga et al., Functional inhibition of hematopoietic and neurotrophic cytokines by blocking the interleukin 6 signal transducer gp130. Proc. Natl. Acad. Sci. U.S.A. 89, 10998–11001 (1992).

54. S. Davis et al., Released form of CNTF receptor alpha component as a soluble mediator of CNTF responses. Science 259, 1736–1739 (1993).

55. O. Robledo et al., Binding interactions of leukemia inhibitory factor and ciliary neurotrophic factor with the different subunits of their high affinity receptors. J. Neurochem. 66, 1391–1399 (1996).

56. J. A. Van Deventer, K. D. Wittrup, Yeast surface display for antibody isolation: Library construction, library screening, and affinity maturation. Methods Mol. Biol. 1131, 151–181 (2014).

57. P. C. Cirino, K. M. Mayer, D. Umeno, Generating mutant libraries using error-prone PCR. Methods Mol. Biol. 231, 3–9 (2003).

58. A. M. Aguinaldo, F. H. Arnold, Staggered extension process (StEP) in vitro recombination. Methods Mol. Biol. 231, 105–110 (2003).

59. J. Yang et al., Improved protein structure prediction using predicted interresidue orientations. Proc. Natl. Acad. Sci. U.S.A. 117, 1496–1503 (2020).